EARTHQUAKE ENGINEERING AND STRUCTURAL DYNAMICS
Earthquake Engng Struct. Dyn. 2000; **29**:213–240

Seismic response of rotating machines–structure–RFBI systems

Wen-Chyi Su, Alan G. Hernried and Solomon C. S. Yim*

Department of Civil, Construction and Environmental Engineering, Oregon State University, Corvallis, OR 97331, U.S.A.

SUMMARY

The seismic response of a critical rotating machine either rigidly attached to a floor or independently isolated housed within an initially aseismically designed or uncontrolled structure are investigated. A particular isolation system, the Resilient-Friction Base Isolator (RFBI), is employed. Finite element formulations of a rotor-disk-bearing model on a rigid base are developed. The equations of motion for the combined rotating machine–structure–RFBI systems are presented. Parametric studies are performed to investigate the effects of variations in system physical properties including friction coefficient, mass ratio, shaft flexibility, bearing rigidity, bearing damping and speed of rotation on the response of rotating machines for the combined rotating machine–structure–isolator systems. Comparative studies in the peak response of the rotating machine supported on various isolation systems and the corresponding fixed base system are carried out. The study indicates that the Resilient-Friction Base Isolator can significantly reduce the seismic response of rotating components to potentially damaging ground excitations. Copyright © 2000 John Wiley & Sons, Ltd.

KEY WORDS: non-linear response; rotating machines; base isolation; resilient-friction isolator

INTRODUCTION

In aseismic design, it is necessary to protect not only the primary structure but also its internal components in the event of severe ground motions. Such non-structural components may serve a critical function, and often are more costly and valuable than the structures themselves. Rotating machines are among the vital internal components of many modern structures. Compressors in ventilation and cooling systems, pumps in power generation facilities, as well as high-speed computers are but a few examples of rotating machinery that must remain functional during and after a severe earthquake.

* Correspondence to: Solomon C. S. Yim, Department of Civil, Construction and Environmental Engineering, Oregon State University, 202 Apperson Hall, Corvalis, Oregon 97331-2302, U.S.A.

Contract/grant sponsor: U.S. National Science Foundation; contract/grant number: CMS-9301464.
Contract/grant sponsor: Department of Civil, Construction and Environmental Engineering at Oregon State University.

Received 17 December 1998
Revised 12 August 1999
Accepted 17 August 1999

CCC 0098-8847/2000/020213-28$17.50
Copyright © 2000 John Wiley & Sons, Ltd

Conventional techniques for designing structures to withstand strong earthquakes can lead to higher floor accelerations in stiff buildings and larger interstorey drifts in flexible structures. These two factors have caused difficulties in insuring the functionality of the building components and equipment. Recent earthquakes have demonstrated that a structure designed in these ways may perform well during a strong earthquake yet still become non-functional due to damages to the critical internal components. For example, in the telephone exchange company in the Sylmar area of California the entire stock of internal rotating equipment was destroyed during the 1971 San Fernando earthquake, but the damage to the building was minor. Another example is the evacuation of several hospitals during the recent Northridge earthquake in the Los Angeles, CA, area which were not caused by structural failure but resulted from the failure of the rotating components described above [1]. Another difficult issue to address from a conventional design viewpoint is that of reducing the internal component and building-content damages. This is very often neglected, and when addressed, can be very expensive to incorporate in conventional design.

An alternative design strategy, aseismic base isolation, is to separate a building from the damaging horizontal components of an earthquake by a base isolation device which prevents or reduces the transmission of horizontal acceleration into the primary structures and their internal components. This new design methodology significantly reduces both floor acceleration and interstorey drift and thus provides a viable economic solution to reducing internal component earthquake damage.

A rotating machine is an inherently very complex system and its analysis for seismic response is equally complex. The complexity of the system is due to the presence of gyroscopic terms and other effects including non-uniform shaft with shear deformation effects. Based on past studies, it is crucial to include the gyroscopic term as it significantly affects the response behaviour [2–6]. Furthermore, the interaction of the machine with its bearing is a complex phenomenon to model for analysis purpose. A general and complex model for rotor-bearing system was considered by Srinivasan and Soni [2, 3]. This analytical model was perhaps the most complete inasmuch as they have included the effects of rotatory inertia, shear deformation, rotor-bearing interaction and the most general description of the base motion input with three translational and three rotational components. Gyroscopic effects and parametric terms caused by the rotation of the base were also included in the formulation. A finite element formulation of the shaft with linear interpolation functions was developed to analyse the response of the rotor. Suarez *et al.* [4] extended the work of Srinivasan and Soni by using non-linear interpolation functions to predict some important dynamic characteristics including instability of the rotating system beyond a certain rotational speed. Suarez *et al.* [4] also showed that several velocity-dependent forcing function terms were neglected in the equations of motion developed by Srinivasan and Soni. Numerical studies conducted by Su [5, 6] and Hernried [6] indicated that the effects of the non-linear parametric terms, which arise due to the rotation of the base, and the non-linear forcing function terms, which appear as the product of input velocities in the equations of motion are insignificant. Su [5] and Su and Hernried [6] also developed the coupled, linear partial differential equations of motion for a uniform symmetric rotating shaft to determine the natural frequency and critical rotating speed analytically. They presented a concise finite element formulation based on a more generalized rotating modal analysis approach. Su [5] also suggested a simple and accurate formulation to modify the stiffness matrix of the rotating system using the method of superposition to include shear-deformation effects.

Seismic base isolation is increasingly being utilized as a practical and economical means to protect the primary structures and their internal components [7–20]. A number of seismic base

Copyright © 2000 John Wiley & Sons, Ltd

isolation mechanisms have been described in an extensive review by Kelly [7, 8]. These devices generally fall into two broad categories: the laminated rubber bearing systems and the frictional types. In this study, attention is focused on a particular frictional isolation system, the Resilient-Friction Base Isolation (RFBI) [9–17]. This isolation system, originally purposed by Mostaghel in the early 1980s, is composed of layers of Teflon coated stainless steel plates, a central rubber core and cover plates. For low level excitations the interfacial friction force serves as a structural fuse, while for moderate to severe earthquakes the Teflon-steel layers dissipate energy and limit the force transmitted to the superstructure. The rubber provides a restoring force for the system to limit the relative displacement. Preliminary laboratory tests [18, 19] of the RFBI system together with computer experiments and analytical results have been implemented at University of California, Berkeley. A number of the RFBI systems have been extensively tested and employed to protect building, nuclear power plant and bridges against strong earthquakes in Europe, Japan, New Zealand and United States.

Recent studies [21, 22] have shown that the RFBI is effective in reducing seismic response in lightweight lump-mass internal components from the corresponding fixed-base case. However, systems containing rotating machines in general cannot be accurately modelled using lump-mass representation due to coupled interaction between the rotating machine, the structure and the base isolator. In this study, the seismic response behaviour of rotating machines supported under various isolated configurations (rotor–structure–RFBI, rotor–RFBI–structure and rotor–RFBI–structure–RFBI) and the corresponding fixed-base ones (rotor–structure) is examined using finite-element modelling of the rotating machines. Sensitivity studies of the peak response of rotating machine to variations in friction coefficient, mass ratio, as well as shaft flexibility, bearing rigidity, bearing damping and speed of rotation are investigated. Of particular interest is whether an isolated structure using the RFBI system would protect critical rotating machines housed within. Should this be the case, then additional aseismic protection for critical rotating machines located in a base-isolated structure may not be necessary.

FINITE ELEMENT FORMULATION OF FLEXIBLE ROTATING MACHINE ON A RIGID BASE

The rotating machine to be considered is the rotor-disk-bearing model of Suarez *et al.* [4]. Finite element equations of motion for the flexible rotating shaft located on the rigid base can be derived using energy methods. The shaft is model as a Bernoulli–Euler beam with a circular cross-section which may vary along the length. It is assumed that the shaft is axially inextensible and shear deformation is negligible. The shaft is spinning with a constant angular velocity about the axial direction. In this study, the non-linear parametric terms in the equations of motion, developed by Suarez *et al.* [4] are neglected, but the gyroscopic term is retained.

To obtain the system equations of motion for the rotating machine, the finite element equations of motion for the flexible shaft, rigid disk and bearing system must be developed. In the following sections, finite element formulations for flexible rotating machines on a rigid base will be presented.

Flexible rotating shaft

The schematic of a rotating shaft mounted on the rigid base is shown in Figure 1. Consider a typical finite element of the flexible rotating shaft of length l. The vectors of displacements

Copyright © 2000 John Wiley & Sons, Ltd

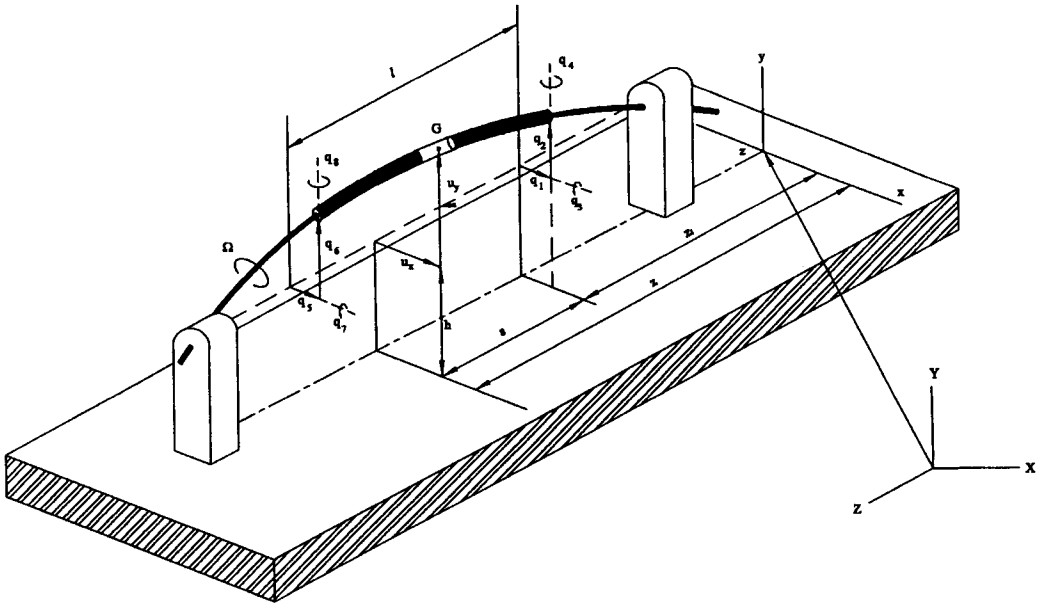

Figure 1. Rotor-bearing system showing nodal co-ordinates and system axes.

and rotations for a typical element and $\mathbf{u}^e$ and $\boldsymbol{\phi}^e$. In the finite-element formulation, these variables can be expressed in terms of the nodal displacements through interpolation functions as

$$\mathbf{u}^e = [u_x^e(s), u_y^e(s), 0]^{\mathrm{T}} = \mathbf{N}\mathbf{q}^e$$

$$\boldsymbol{\phi}^e = [\theta_x^e(s), \theta_y^e(s), 0]^{\mathrm{T}} = \mathbf{N}'\mathbf{q}^e \tag{1}$$

where $\mathbf{q}^e$ is a vector of nodal displacements; s is a local co-ordinate measured along the length of a finite element; $\mathbf{N}$ is the matrix of interpolation functions; $\mathbf{N}'$ is the first derivation of $\mathbf{N}$ with respect to s.

By direct application of the energy method (Lagrange formulation), the finite-element equations of motion for the flexible rotating shaft can be obtained as

$$\mathbf{M}_s^e\ddot{\mathbf{q}}^e + \mathbf{C}_s^e\dot{\mathbf{q}}^e + \mathbf{K}_s^e\mathbf{q}^e = \mathbf{f}_s^e(\ddot{x}_g(t), \ddot{y}_g(t)) \tag{2}$$

where the element mass, damping, stiffness and applied force matrices are defined by

$$\mathbf{M}_s^e = \int_0^l \rho A\mathbf{N}^{\mathrm{T}}\mathbf{N}\,\mathrm{d}s + \int_0^l \rho I_x\mathbf{N}'^{\mathrm{T}}\mathbf{N}'\,\mathrm{d}s \tag{3a}$$

$$\mathbf{C}_s^e = \Omega\int_0^l I_p\mathbf{N}'^{\mathrm{T}}(\mathbf{e}_1\mathbf{e}_2^{\mathrm{T}} - \mathbf{e}_2\mathbf{e}_1^{\mathrm{T}})\mathbf{N}'\,\mathrm{d}s \tag{3b}$$

Copyright © 2000 John Wiley & Sons, Ltd

$$\mathbf{K}_s^e = \int_0^l EI_x \mathbf{N}''^{\mathrm{T}} \mathbf{N}'' \, \mathrm{d}s \tag{3c}$$

$$\mathbf{f}_s^e(\ddot{x}_g, \ddot{y}_g) = -\left[\int_0^l \rho A \mathbf{N}^{\mathrm{T}} \, \mathrm{d}s\right] \mathbf{a}_b(t) \tag{3d}$$

The operational vectors $\mathbf{e}_1$ and $\mathbf{e}_2$ are defined as

$$\mathbf{e}_1 = \begin{bmatrix} 1 \\ 0 \\ 0 \end{bmatrix}, \quad \mathbf{e}_2 = \begin{bmatrix} 0 \\ 1 \\ 0 \end{bmatrix}$$

and ρ = mass density; A = cross-sectional area; I_x and I_p = moments of inertia of shaft about the transverse and normal axes, respectively; Ω = constant speed of rotation; E = Young's modulus; $\ddot{x}_g$ and $\ddot{y}_g$ are horizontal and vertical components of the ground excitation, respectively; and $\mathbf{a}_b(t) = [\ddot{x}_g, \ddot{y}_g, 0]^{\mathrm{T}}$. Note the presence of the gyroscopic term of the flexible rotating shaft (the second term in Equation (3a)).

To satisfy continuity requirements, the interpolation functions in the above equations must be assumed continuous in displacement and slope on the element boundaries. i.e. C' continuity. Thus appropriate nodal quantities are displacements and rotations at each end of the element. The cubic beam (Hermite) polynomials satisfy C' continuity and are an appropriate one for the interpolation function $\mathbf{N}$. The matrix of the cubic interpolation function $\mathbf{N}$ is given by

$$\mathbf{N} = \begin{bmatrix} n_1 & 0 & n_2 & 0 & n_3 & 0 & n_4 & 0 \\ 0 & n_1 & 0 & n_2 & 0 & n_3 & 0 & n_4 \\ 0 & 0 & 0 & 0 & 0 & 0 & 0 & 0 \end{bmatrix} \tag{4}$$

where

$$n_1 = 1 - \frac{3s^2}{l^2} + \frac{2s^3}{l^3}, \quad n_3 = \frac{3s^2}{l^2} - \frac{2s^3}{l^3}$$
$$n_2 = s - \frac{2s^2}{l} + \frac{s^3}{l^2}, \quad n_4 = \frac{s^3}{l^2} - \frac{s^2}{l} \tag{5}$$

Each element has two nodes, one at each end of the element. As shown in Figure 2, there are four degrees of freedom at each node, two transitional degrees of freedom (u_x^e, u_y^e) and two rotational degrees of freedom (θ_x^e, θ_y^e) in the x- and y-directions. Therefore, $\mathbf{q}^e$ in Equation (2) is a 8×1 vector of nodal displacements and rotations given by

$$\mathbf{q}^e = [u_{x1}^e, u_{y1}^e, \theta_{x1}^e, \theta_{y1}^e, u_{x2}^e, u_{y2}^e, \theta_{x2}^e, \theta_{y2}^e]^{\mathrm{T}} \tag{6}$$

where the second subscripts 1 and 2 on the nodal displacement variable pertain to the left and right ends of the elements, respectively.

Rigid disk

The rotating machine considered may contain several rigid disks along the shaft. To include the effects of these disks on the response of the flexible shaft, they can be modelled as thin rigid disks with concentrated mass attached at the finite-element nodes.

Copyright © 2000 John Wiley & Sons, Ltd

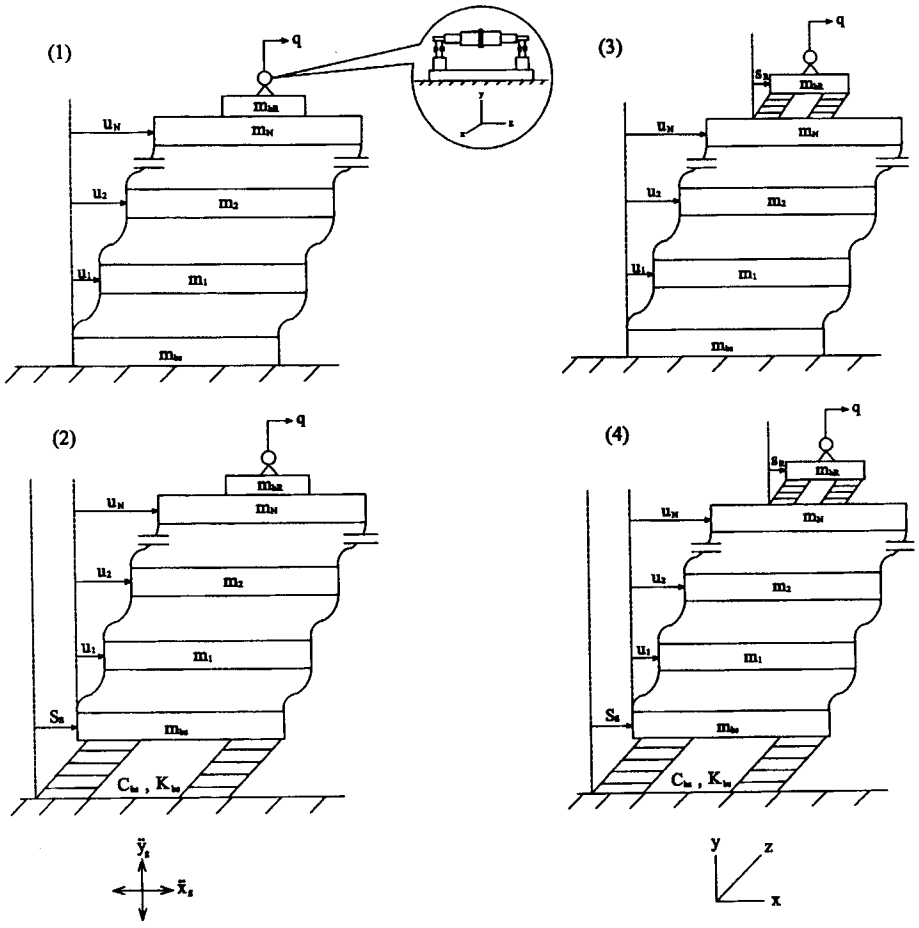

Figure 2. Schematic diagrams of the combined rotor–structure–RFBI systems.

The displacements and rotations at an arbitrary point in a typical element of the shaft are given in Equation (1). Without loss of generality, assume a rigid disk is attached at the left end ($s = 0$ location) of a typical element. Since the disk is attached to only one end of the element, the quantities of Equation (6) can be rewritten as

$$\mathbf{u}_{\mathrm{d}}^{e} = \mathbf{u}^{e}(s = 0) = \mathbf{A}\mathbf{q}_{\mathrm{d}}^{e} \tag{7}$$

where

$$\mathbf{A} = \begin{bmatrix} 1 & 0 & 0 \\ 0 & 1 & 0 \\ 0 & 0 & 0 \end{bmatrix}, \quad \mathbf{q}_{\mathrm{d}}^{e} = [u_x, u_y, \theta_x, \theta_y]^{\mathrm{T}} \tag{8}$$

The internal bending strain energy associated with the rigid disk is zero. Neglecting the potential energy term in the Lagrange formulation, the equations of motion for a rigid disk can be

Copyright © 2000 John Wiley & Sons, Ltd

obtained directly in a manner similar to those for the flexible shaft, resulting in

$$\mathbf{M}_{\mathrm{d}}^{e}\ddot{\mathbf{q}}^{e} + \mathbf{C}_{\mathrm{d}}^{e}\dot{\mathbf{q}}^{e} + \mathbf{K}_{\mathrm{d}}^{e}\mathbf{q}^{e} = \mathbf{f}_{\mathrm{d}}^{e}(\ddot{x}_{\mathrm{g}}, \ddot{y}_{\mathrm{g}}) \tag{9}$$

In the above equation, the mass, damping, stiffness and applied force matrices are

$$\mathbf{M}_{\mathrm{d}}^{e} = m_{\mathrm{d}}\mathbf{A}^{\mathrm{T}} + \mathbf{A} + I_{\mathrm{t}}\mathbf{A}'^{\mathrm{T}}\mathbf{A}' \tag{10a}$$

$$\mathbf{C}_{\mathrm{d}}^{e} = \Omega I_{\mathrm{o}}\mathbf{A}'^{\mathrm{T}}[\mathbf{e}_1\mathbf{e}_2^{\mathrm{T}} - \mathbf{e}_2\mathbf{e}_1^{\mathrm{T}}]\mathbf{A}' \tag{10b}$$

$$\mathbf{K}_{\mathrm{d}}^{e} = \mathbf{0} \tag{10c}$$

$$\mathbf{f}_{\mathrm{d}}^{e}(\ddot{x}_{\mathrm{g}}, \ddot{y}_{\mathrm{g}}) = -m_{\mathrm{d}}\mathbf{A}^{\mathrm{T}}\mathbf{a}_{\mathrm{b}}(t) \tag{10d}$$

where m_{d} is the mass of disk; I_{t} and I_{o} are the mass moments of inertia of disk about transverse and normal axes, respectively. Note the presence of the gyroscopic term of the rigid disk (the second term in Equation (10a)).

Journal-fluid-bearing system

The bearing system provides stiffness as well as desirable damping for the rotating machine. The stiffness and damping properties of the bearing directly affect the critical speeds and the stability of the rotor. Fluid-film bearings are generally modelled by two orthogonal (linear elastic and damping) forces. These forces depend on the displacements and velocities at the bearing location, respectively [23]. The damping forces in the transverse directions are coupled and the elements of the damping matrix are symmetric; while the elastic forces in the transverse directions are coupled but the elements of the stiffness matrix are asymmetric. Several references in the literature [23–27] provide methods to obtain the coefficients of the damping and stiffness matrices. These coefficients depend upon the type of bearing, its physical dimension, the viscosity of the fluid and the rotating speed of the rotor. In this study, the stiffness and damping characteristics of the bearing with $L/D = 1$ are provided by Earles and Palazzolo [24].

$$C_{ij}^{\mathrm{b}} = Wc_{ij}/h, \quad K_{ij}^{\mathrm{b}} = Wk_{ij}/h \tag{11}$$

where W, h, D and L are the weight on bearing, radial clearance, journal diameter and bearing length, respectively; the subscripts i and j correspond to directions x and y, respectively; k_{ij} and c_{ij} are

$$\begin{aligned} k_{xx} &= 1.512 - 3.218s_f + 0.889s_f^2, \quad k_{xy} = -0.73 + 18.217s_f + 1.67s_f^2 \\ k_{yx} &= -2.677 - 8.675s_f - 3.658s_f^2, \quad k_{yy} = 3.61 + 15.962s_f + 5.87s_f^2 \end{aligned} \tag{12a}$$

and

$$\begin{aligned} c_{xx} &= 0.822 + 13.051s_f - 0.528s_f^2, \quad c_{xy} = -2.764 + 23.949s_f - 1.755s_f^2 \\ c_{yx} &= -2.764 + 23.949s_f - 1.755s_f^2, \quad c_{yy} = 4.31 + 43.087s_f + 6.18s_f^2 \end{aligned} \tag{12b}$$

where s_f is the Summerfield number defined as

$$s_f = \frac{\mu\Omega DL}{W}\left(\frac{R}{h}\right)^2 \tag{12c}$$

Copyright © 2000 John Wiley & Sons, Ltd

where μ and R are lubricant viscosity and journal radius, respectively. Therefore, the fluid-film reaction force, damping and stiffness matrices of the bearing, corresponding to the displacement and velocity vectors of a node, can be expressed in the following form:

$$\mathbf{K}_b^e = \begin{bmatrix} k_{xx} & k_{xy} & 0 \\ k_{yx} & k_{yy} & 0 \\ 0 & 0 & 0 \end{bmatrix}; \quad \mathbf{C}_b^e = \begin{bmatrix} c_{xx} & c_{xy} & 0 \\ c_{yx} & c_{yy} & 0 \\ 0 & 0 & 0 \end{bmatrix} \tag{13}$$

System equations of motion

In order to obtain the system equations of motion, a direct stiffness method to assemble the element mass, damping, stiffness and applied forces matrices will be used. The system matrices are constructed simply by adding terms from the individual element matrices into their corresponding locations in the global matrices. The system mass, damping, stiffness and applied force matrices are

$$\begin{gathered} \mathbf{M}^R = \mathbf{M}_s^e + \mathbf{M}_d^e, \quad \mathbf{C}^R = \mathbf{C}_s^e + \mathbf{C}_d^e + \mathbf{C}_b^e \\ \mathbf{K}^R = \mathbf{K}_s^e + \mathbf{K}_d^e + \mathbf{K}_b^e, \quad \mathbf{f}^R(t) = \mathbf{f}^R(t) + \mathbf{f}_d^e(t) \end{gathered} \tag{14}$$

and the generalized coordinates $\mathbf{q}$ for the system are

$$\mathbf{q} = [u_{x1}, u_{y1}, \theta_{x1}, \theta_{y1}, \ldots, u_{x4(n-1)}, u_{y4(n-1)}, \theta_{x4(n-1)}, \theta_{y4(n-1)}]^T \tag{15}$$

where n is the total number of nodes in the system

EQUATIONS OF MOTION OF COMBINED ROTATING MACHINE–STRUCTURE–ISOLATOR SYSTEMS

In this section, the governing equations of motion for the rotating machine either rigidly attached to a floor level or independently isolated within an aseismically designed or uncontrolled structure are presented. To determine the efficiency and economy of the isolated systems in protecting the internal rotating components, four combined rotating machine–structure-isolator models are examined. The schematic diagrams of these models are shown in Figure 2 and discussed below. A flexible rotating machine is assumed to be:

(1) rigidly attached to a floor level in a non-isolated multistorey building (rotor–structure),
(2) rigidly attached to a floor level in a base-isolated multistorey building (rotor–structure–RFBI),
(3) supported on isolators which are rigidly attached to a floor level in a non-isolated multistorey building (rotor–RFBI–structure), and
(4) supported on isolators which are rigidly attached to a floor level in a base-isolated multistorey building (rotor–RFBI–structure–RFBI).

By applying Newton's Law, the governing equations of motion for a flexible rotating machine supported on a RFBI system which are rigidly attached to a floor level in a base isolated

Copyright © 2000 John Wiley & Sons, Ltd

multistorey building (rotor-RFBI-structure-RFBI) are governed by

$$\ddot{s}_R + 2\xi_{bR}\omega_{bR}\dot{s}_R + \omega_{bR}^2 s_R = -(\ddot{x}_g + \ddot{s}_s + \ddot{u}_N) - \mu_R \operatorname{sgn}(\dot{s}_R)\left(g + \ddot{y}_g + \sum_{i=4k-2}^{n-2}\sum_{j=1}^{n}\beta_{ij}^R \ddot{q}_j\right) - \sum_{i=4k-3}^{n-3}\sum_{j=1}^{n}\gamma_{ij}^R \ddot{q}_j \tag{16a}$$

$$\ddot{s}_s + 2\xi_{bs}\omega_{bs}\dot{s}_s + \omega_{bs}^2 s_s = -\ddot{x}_g - \mu_s \operatorname{sgn}(\dot{s}_s)\left(g + \ddot{y}_g + \sum_{i=4k-2}^{n-2}\sum_{j=1}^{n}\beta_{ij}^R \ddot{q}_j\right) - \sum_{i=4k-3}^{n-3}\sum_{j=1}^{n}\gamma_{ij}^R \ddot{q}_j - \sum_{i=1}^{p}\alpha_i^s \ddot{u}_i - \sigma(\ddot{u}_N + \ddot{s}_R) \tag{16b}$$

$$\mathbf{M}^s\ddot{\mathbf{u}} + \varepsilon_{iN}\mathbf{C}^s\dot{\mathbf{u}} + \varepsilon_{iN}\mathbf{K}^s\mathbf{u} = -\mathbf{M}^s\mathbf{r}(\ddot{x}_g + \ddot{s}_s) - \delta_{iN}\mathbf{M}^s\mathbf{r}\left(\psi\ddot{s}_R \sum_{i=4k-3}^{n-3}\sum_{j=1}^{n}\gamma_{ij}^f \ddot{q}_j\right) \tag{16c}$$

$$\mathbf{M}^R\ddot{\mathbf{q}} + \mathbf{C}^R\dot{\mathbf{q}} + \mathbf{K}^R\mathbf{q} = -\mathbf{f}^R(\ddot{x}_g, \ddot{y}_g, \ddot{s}_R, \ddot{s}_s, \ddot{u}_N) \tag{16d}$$

where the functions ε_{iN} and δ_{iN} are defined as

$$\varepsilon_{iN} = \begin{cases} 1 & (i \neq N), \\ \dfrac{m_N}{m_R + m_{bR} + m_N} & (i = N), \end{cases} \qquad \delta_{iN} = \begin{cases} 0 & (i \neq N) \\ 1 & (i = N) \end{cases} \tag{16e}$$

The symbols s_R and s_s are the relative sliding displacements of the rotating system base mat relative to the floor level and building base mat relative to the ground, respectively; g is the gravitational acceleration; $\mathbf{r}$ is a unit vector; $\mathbf{u}$ is the relative displacement vector between a floor level and the building base mat; μ_R and μ_s are the friction coefficients of the isolators of the rotating machine and building, respectively. The mass, damping and stiffness matrices of the rotating machine are expressed as $\mathbf{M}^R$, $\mathbf{C}^R$ and $\mathbf{K}^R$, respectively, while the mass, damping and stiffness matrices of the multistorey building are $\mathbf{M}^s$, $\mathbf{C}^s$ and $\mathbf{K}^s$, respectively. The applied forcing function $\mathbf{f}^R$ is slightly modified, because the element vector of transitional base acceleration $\mathbf{a}_b(t)$ in Equations (3d) and (10d) is replaced by $[(\ddot{x}_g + \ddot{s}_R + \ddot{s}_s + \ddot{u}_N), \ddot{y}_g, 0]^T$. The subscript k and the upper limit of the summation n are the total number of nodes and the total degrees of freedom of the rotating shaft. The subscript N and the upper limit of the summation p indicate the specified floor of the multistorey building where the rotating machine is located, and the total number of floors in the multistorey building, respectively. According to the definition of the generalized coordinates $\mathbf{q}$ in Equation (15), the mass of the kth rotating shaft element corresponding to coordinate x- and y-directions due to acceleration of co-ordinate j can be expressed as $m_{(4k-3)j}^R$ and $m_{(4k-2)j}^R$, respectively. The coefficients γ_{ij}^s, β_{ij}^s, α_i^s, σ, ψ are the sign functions $\operatorname{sgn}(\dot{s}_R)$, $\operatorname{sgn}(\dot{s}_s)$ are defined as

$$M_t = m_R + m_{bR} + m_{bs} + \sum_{i=1}^{p} m_i$$

$$\gamma_{ij}^s = \frac{m_{(4k-3)j}^R}{M_t}, \quad \gamma_{ij}^f = \frac{m_{(4k-3)j}^R}{m_R + m_{bR} + m_N}, \quad \beta_{ij}^s = \frac{m_{(4k-2)j}^R}{M_t} \tag{17}$$

$$\alpha_i = \frac{m_i}{M_t}, \quad \sigma = \frac{m_R + m_{bR}}{M_t}, \quad \psi = \frac{m_{(4k-3)j}^R}{m_R + m_{bR} + m_N}$$

Copyright © 2000 John Wiley & Sons, Ltd

and

$$\operatorname{sgn}(\dot{s}_R) = \begin{cases} +1 & \dot{s}_R > 0 \\ -\dfrac{\ddot{x}_g + \ddot{s}_s + \ddot{u}_N + \omega_{bR}^2 s_R + \sum_{i=4k-3}^{n-3} \sum_{j=1}^{n} \gamma_{ij}^R \ddot{q}_j}{\mu_R (g + \ddot{y}_g + \sum_{i=4k-2}^{n-2} \sum_{j=1}^{n} \beta_{ij}^R \ddot{q}_j)} & \dot{s}_R = \ddot{s}_R = 0 \\ -1 & \dot{s}_R < 0 \end{cases} \tag{18a}$$

$$\operatorname{sgn}(\dot{s}_s) = \begin{cases} +1 & \dot{s}_s > 0 \\ -\dfrac{\ddot{x}_g + \omega_{bs}^2 s_s + \sum_{i=4k-3}^{n-3} \sum_{j=1}^{n} \gamma_{ij}^s \ddot{q}_j + \sum_{i=1}^{p} \alpha_i \ddot{u}_i + \sigma(\ddot{u}_N + \ddot{s}_R)}{\mu_s (g + \ddot{y}_g + \sum_{i=4k-2}^{n-2} \sum_{j=1}^{n} \beta_{ij}^s \ddot{q}_j)} & \dot{s}_s = \ddot{s}_s = 0 \\ -1 & \dot{s}_s < 0 \end{cases} \tag{18b}$$

where m_R, m_{bR}, m_{bs} and m_i are the masses of the rotating machine, rotating-system base mat, building base mat and the mass of ith floor, respectively. The natural circular frequencies of the rotating system base and building base, and their effective damping ratios are defined as

$$2\xi_{bR}\omega_{bR} = \frac{c_{bR}}{m_R + m_{bR}}, \quad \omega_{bR}^2 = \frac{k_{bR}}{m_R + m_{bR}}, \quad 2\xi_{bs}\omega_{bs} = \frac{c_{bs}}{M_t}, \quad \omega_{bs}^2 = \frac{k_{bs}}{M_t} \tag{19}$$

where c_{bR}, c_{bs}, k_{bR} and k_{bs} are the damping and the horizontal stiffness coefficients of the isolators of the rotating machine and multistorey building, respectively.

Deformations of the structure and the rotating machine are governed by Equations (16c) and (16d), respectively. These equations are coupled with Equations (16a) and (16b) through the inertial forces. Equation (16a) governs both the sliding and non-sliding phases of the RFBI of the rotating system. A similar criterion of transition has been described earlier. The non-sliding phase of the rotating system continues as long as

$$\left| \ddot{x}_g + \ddot{s}_s + \ddot{u}_N + \omega_{bR}^2 s_R + \sum_{i=4k-3}^{n-3} \sum_{j=1}^{n} \gamma_{ij}^R \ddot{q}_j \right| < \mu_g \left(g + \ddot{y}_g + \sum_{i=4k-2}^{n-2} \sum_{j=1}^{n} \beta_{ij}^R \ddot{q}_j \right) \tag{20a}$$

As soon as the condition,

$$\left| \ddot{x}_g + \ddot{s}_s + \ddot{u}_N + \omega_{bR}^2 s_R + \sum_{i=4k-3}^{n-3} \sum_{j=1}^{n} \gamma_{ij}^R \ddot{q}_j \right| = \mu_g \left(g + \ddot{y}_g + \sum_{i=4k-2}^{n-2} \sum_{j=1}^{n} \beta_{ij}^R \ddot{q}_j \right) \tag{20b}$$

is satisfied, sliding motion of the rotating system starts and the direction of sliding is given by Equation (19a) with $\dot{s}_R = \ddot{s}_R = 0$. When the rotating machine is not sliding, $\ddot{s}_R = \dot{s}_R = 0$, the motion is governed by Equations (16b)–(16d) with $\ddot{s}_R = \dot{s}_R = s_R = 0$, which is the case rotor–structure–RFBI.

Similarly, Equation (16b) governs both the sliding and non-sliding phases of the building. The non-sliding phase of the building continues as long as

$$\left| \ddot{x}_g + \omega_{bs}^2 s_s + \sum_{i=4k-3}^{n-3} \sum_{j=1}^{n} \gamma_{ij}^R \ddot{q}_j + \sum_{i=1}^{p} \alpha_i \ddot{u}_i + \sigma(\ddot{u}_N + \ddot{s}_R) \right| < \mu_R \left(g + \ddot{y}_g + \sum_{i=4k-2}^{n-2} \sum_{j=1}^{n} \beta_{ij}^R \ddot{q}_j \right) \tag{21a}$$

Copyright © 2000 John Wiley & Sons, Ltd

As soon as the condition,

$$\left| \ddot{x}_g + \omega_{bs}^2 s_s + \sum_{i=4k-3}^{n-3} \sum_{j=1}^{n} \gamma_{ij}^R \ddot{q}_j + \sum_{i=1}^{p} \alpha_i \ddot{u}_i + \sigma(\ddot{u}_N + \ddot{s}_R) \right| = \mu_R \left(g + \ddot{y}_g + \sum_{i=4k-2}^{n-2} \sum_{j=1}^{n} \beta_{ij}^R \ddot{q}_j \right) \quad (21b)$$

is satisfied, sliding motion of the building starts and the direction of sliding is given by Equation (18b) with $\dot{s}_s = \ddot{s}_s = 0$. When the structural system is not sliding, $\ddot{s}_s = \dot{s}_s = 0$, the motion is governed by Equations (16a), (16c) and (16d) with $\ddot{s}_s = 0$, which is the case of rotor–RFBI–structure.

When the rotating machine and the structural system both are not sliding, i.e., $\ddot{s}_R = \dot{s}_R = 0$ and $\ddot{s}_s = \dot{s}_s = 0$, the motion is governed by Equations (16c) and (16d) with $\ddot{s}_s = 0$ and $\ddot{s}_R = \dot{s}_R = s_R = 0$, which is the case of the rotor-structure.

PARAMETRIC STUDY

As an example of the seismic analysis of the machine, structure and RFBI system, a stable rotating machine is shown in Figure 3. The physical properties of this model are provided in Table I. The rotor is modelled using 14 infinite elements with a total of 60 degrees of freedom. The bearing system has stiffness and damping coefficients given by Lund and Tomsen [26] for elliptical bearings with $L/D = 1$. A simple linear three-storey building with identical mass, column damping and column stiffness at various storeys is employed as the structural model. The schematic diagrams of the combined rotating machine–structure–isolator systems are shown in Figure 2.

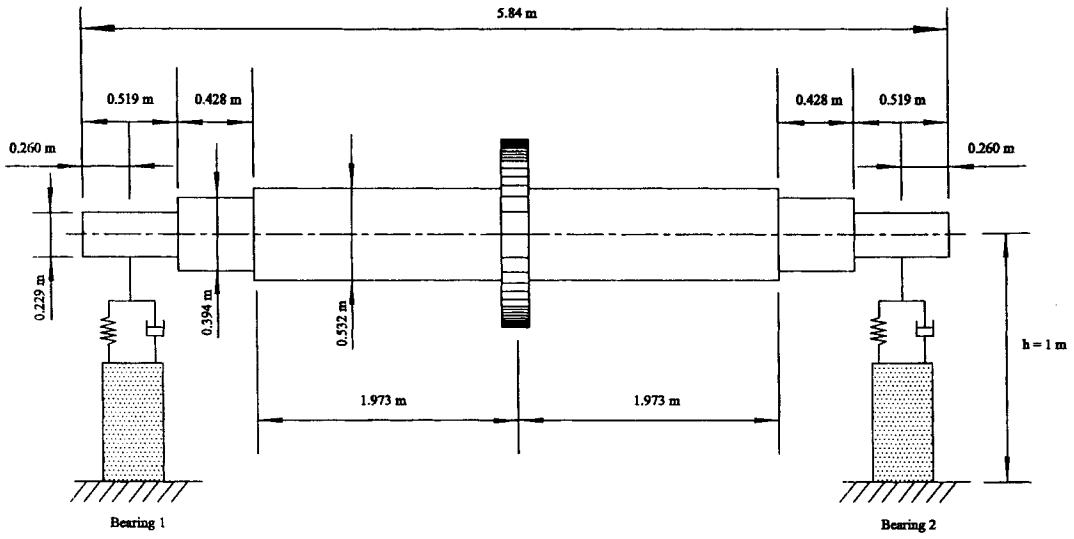

Figure 3. Schematic of a rotor-disk-bearing model on rigid base considered for seismic study.

Copyright © 2000 John Wiley & Sons, Ltd

Table I. Physical and mechanical properties of the rotating machine.

Shaft	*Rotor disk*
Modulus of elasticity, $E = 2.078 \times 10^{11}$ N/m^2	Disk mass $m_d = 5670$ kg
Mass density, $\rho = 7806$ kg/m^2	Transverse moment of inertia, $I_x = 3550$ kg m^2
Poisson's ratio, $\nu = 0.3$	Polar moment of inertia, $I_p = 7100$ kg m^2
Revolutions per minute, $\Omega = 880$ rpm	
Bearing system	
Viscosity $\mu = 0.14839$ N s/m^2	Clearance, $C = 3.8 \times 10^{-4}$
Diameter of journal, $D = 0.229$ m	Weight on bearing $W = 67120$ N
Length of journal, $L = 0.229$ m	L/D ratio $= 1.0$

In order to predict the absolute maximum response of the rotating machine in the combined rotating machine–structure–isolator systems, the rotating machine is assumed to be located at the top floor of the structure. The response of the rigid disk corresponding to the sliding direction is calculated to represent the response of the complete rotating system. The first 20 s of the N–S and the vertical components of the El Centro 1940 earthquake are used simultaneously as the ground-excitation input in the sensitivity study presented below.

A numerical step-by-step time integration scheme, the Newmark-β [28] method, is employed in this parametric study. The response of the RFBI system is found to be sensitive to the times of transition between the sliding and non-sliding phases. Precise evaluation of the time of phase transitions is crucial to accurate prediction of the response. To assure convergence of the predictions, a time step of $\Delta t = 2 \times 10^{-4}$ s is used during the continuous phases of motion away from the phase transitions; and $\Delta t = 2 \times 10^{-5}$ s is employed near the times of phase transition and the times when sliding changes direction [9]. In the computations, sliding velocities of the RFBI system less than 0.01 mm/s are assumed to be zero. Based on the numerical study conducted here, using these time steps and transition criterion is sufficient to achieve convergence in the prediction of the non-linear dynamic response.

In the subsequent analysis, the rotating machine is operated at a constant angular velocity of 880 rpm. The structural period T_s is varied between 0.1 and 2.0 s to cover the range of stiff to flexible structures. The recommended natural period T_b of 4.0 s is used for the RFBI system. The damping ratios of the structure, ξ_s, and the base for the rotating machine and structure ξ_{bR}, ξ_{bs} are 0.04, 0.08 and 0.08, respectively. The mass ratios of the rotating-machine mat, floor and structural mat to the rotating machine, m_{bR}/m_R, m_i/m_R, m_{bs}/m_R, of 1, 2 and 3 are specified, respectively. Unless stated otherwise these values are employed throughout the parametric study.

Effects of varying friction coefficient

The effect of variations in the friction coefficient of the various base-isolated systems on the peak absolute disk acceleration response $(\ddot{x}_g + \ddot{u}_3 + \ddot{q} + \ddot{s}_s + \ddot{s}_R)_{max}$ and the peak sliding displacement of the machine base mat $(s_R)_{max}$ are investigated. The peak acceleration and peak sliding displacement responses with respect to the friction coefficient are plotted against the structural period T_s and shown in Figures 4 and 5, respectively. Corresponding responses of the fixed-base systems are also plotted in the figures for comparison. A range of friction coefficients μ_s and μ_R, from 0.01 to 0.2 is used.

Copyright © 2000 John Wiley & Sons, Ltd

Figures 4(a)–(c) show that the level of peak disk acceleration responses of the combined rotor–structure–RFBI systems (rotor–structure–RFBI, rotor–RFBI–structure and rotor–RFBI–structure–RFBI) are, in general, considerably lower than those of the corresponding fixed-base ones. The smaller the friction coefficient, the great the reduction in the disk responses.

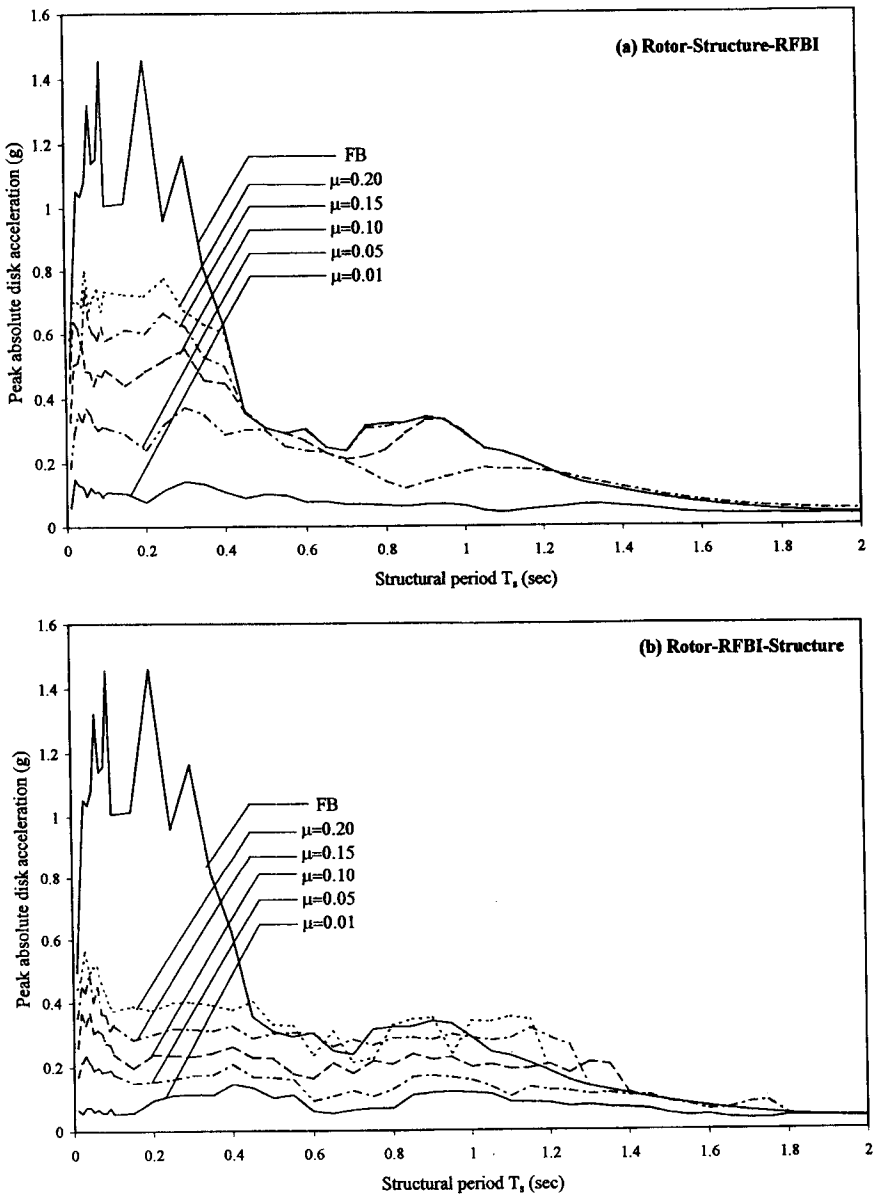

Figure 4. Effect of friction coefficient on disk acceleration response.

Copyright © 2000 John Wiley & Sons, Ltd

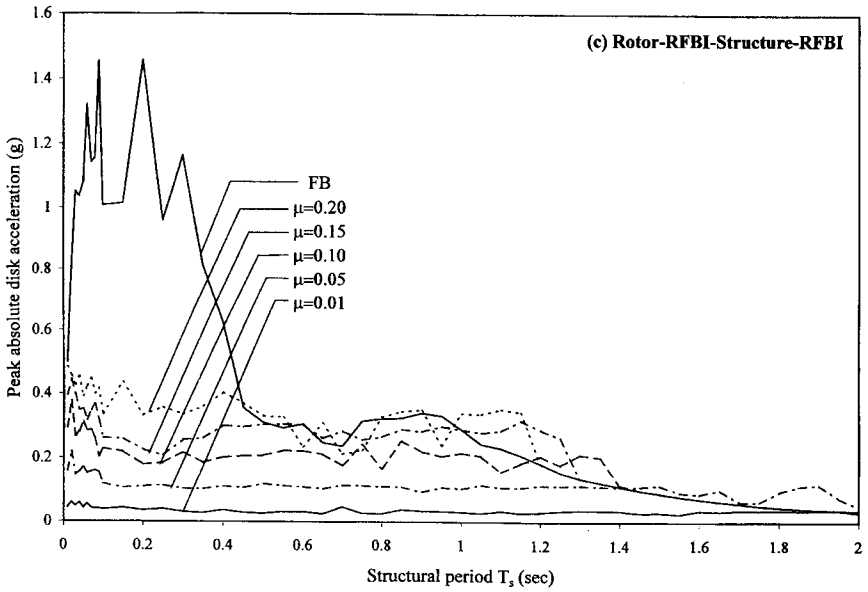

Figure 4. *Continued.*

In addition, the spectral response of the base-isolated systems appears to be almost independent of the frequency of excitation, especially for the smaller friction coefficients of the RFBI system. The response spectra of the fixed-base cases contain several dominate peaks that indicate significant energy transmitted into the rotating machine at these particular frequencies. When the dominant frequencies of the rotating machine are tuned to the structural natural frequency, large amplification in the disk response occurs due to the resonant effect. In the large amplitude region (tuning region), the various isolated systems, especially the rotor–RFBI–structure system, are extremely effective in reducing the response of the rotating machine when the systems are subjected to strong ground motions such as the El Centro record. In the higher structural period region ($T_s > 1.0$ s), there is relatively little change in the response of the rotating machine in the isolated systems as compared to the fixed-base case.

From Figure 4, it is observed that there are several exceptions where the disk acceleration responses in the isolated systems exceed those in their corresponding fixed-base ones, especially in the relatively large friction coefficient case. These occur at $\mu_R = 0.20$ and $T_s = 0.45$–0.55, 0.8–1.2 s; $\mu_R = 0.15$ and $T_s = 0.6$, 1.0–1.3 s for the rotor–RFBI–structure model. Similar exceptions occur at $\mu_R = \mu_s = 0.20$ and 0.15 for the rotor–RFBI–structure–RFBI models. This is due to the non-linear stick-slip and slip-reversal transitions (i.e., stick-slip friction action) of the RFBI system imparting significant energy into the rotating machine. In addition, the interaction between the rotating machine and its isolator contributes significantly to the amplifications in the disk response if the masses of the rotating machine and its base are relatively large. However, amplifications in these particular ranges could be reduced as the friction coefficient is decreased, but it should be chosen such that it could prevent any sliding under low level excitations. Furthermore, the rotor–RFBI–structure–RFBI system has better performance in reducing the peak disk response than the others in the high amplification period range ($T_s < 0.5$ s).

Copyright © 2000 John Wiley & Sons, Ltd

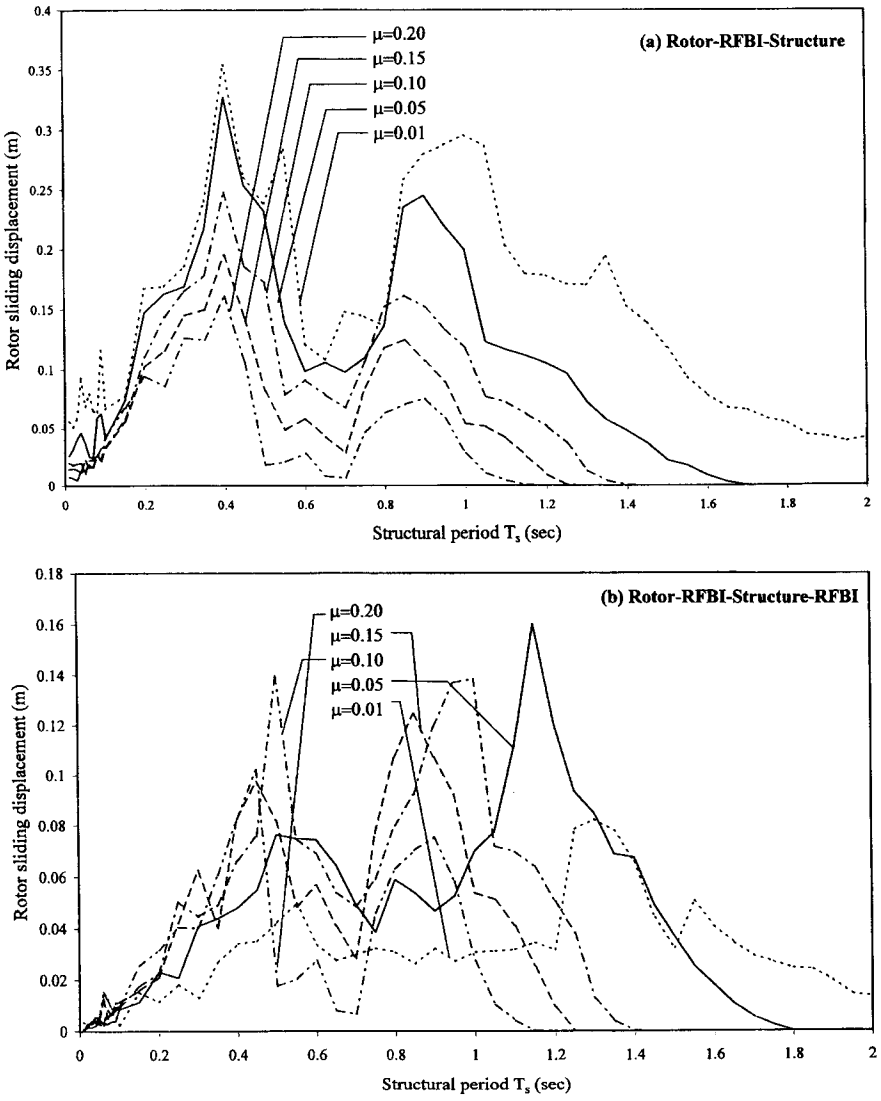

Figure 5. Effect of friction coefficient on sliding displacement response of rotating system.

Figures 5(a) and (b) show the peak sliding displacement response spectra of the rotating machine for the rotor–RFBI–structure and rotor–RFBI–structure–RFBI models, respectively. For the spectra of the rotor–RFBI–structure model, in general, the maximum response of the sliding displacement of the rotating machine decreases with increasing friction coefficient. This observation is consistent with that of a multistorey building supported on an RFBI subjected to harmonic excitation as reported by Mostaghel *et al.* [29]. This is due to the fact that the input motion at the support of the RFBI of the rotating machine resembles that of a harmonic excitation because the structure serves as a narrow-band linear filter to the random earthquake

Copyright © 2000 John Wiley & Sons, Ltd

excitations. However, for the peak sliding displacement response of the rotating machine of the rotor–RFBI–structure–RFBI model, the maximum response appears to vary randomly, i.e. no systematic trend can be observed. This high degree of randomness may be caused by the non-linear stick-slip friction action, which has significant energy at the high frequency range,

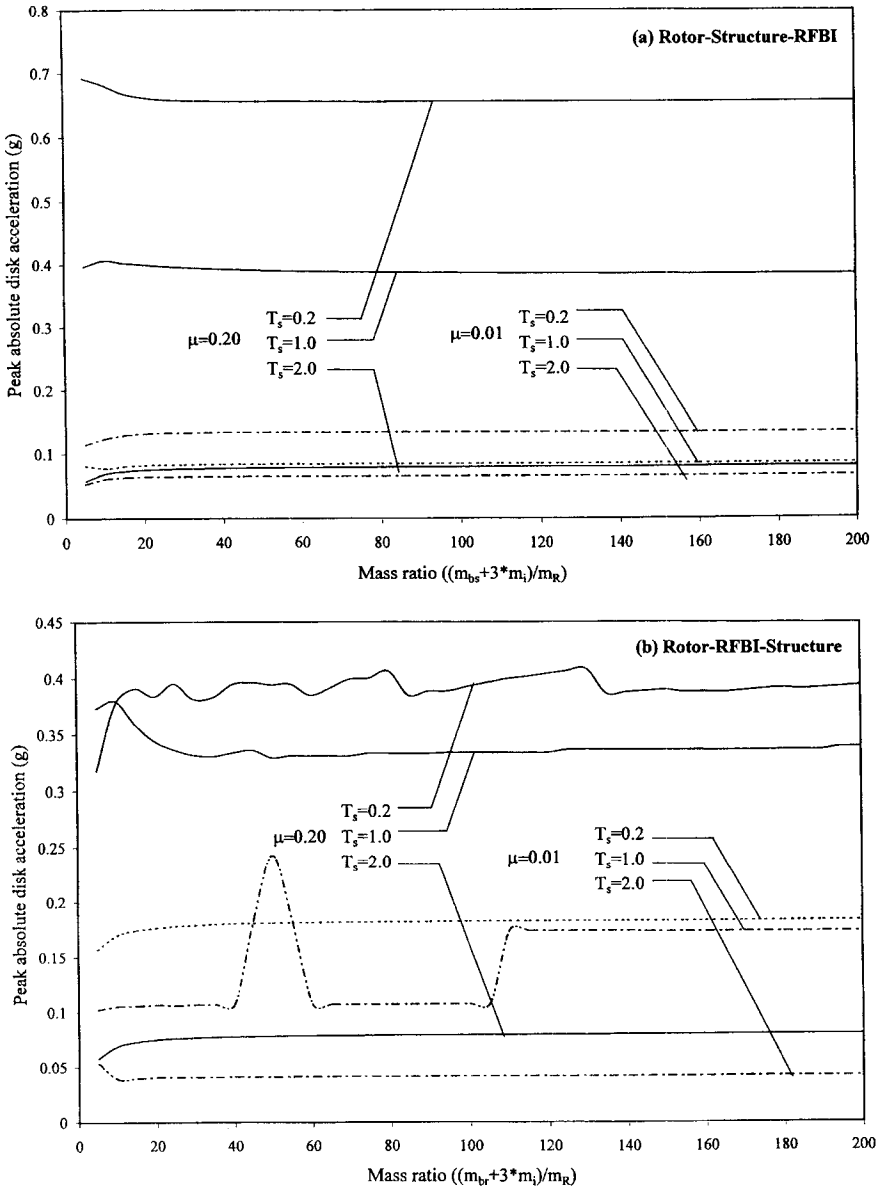

Figure 6. Effect of mass ratio on disk acceleration response.

Copyright © 2000 John Wiley & Sons, Ltd

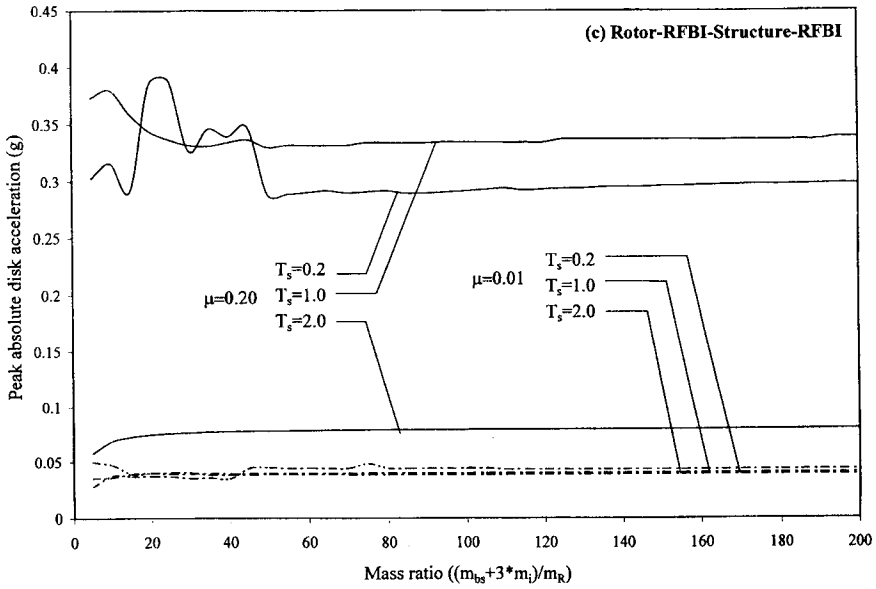

Figure 6. *Continued.*

for the structural base isolator. In addition, the sliding displacement, which may result in a permanent offset between the sliding parts after an earthquake, is a possible major disadvantage for the most frictional type base isolation. However, it can be observed that the sliding displacements are insignificant and may be neglected in most instances.

Effects of varying mass ratio

The effect of variations in the structure/rotating machine mass ratio $((m_{bs} + \sum_i m_i)/m_R)$ on the peak disk acceleration response for the combined rotating machine–structure–RFBI systems is shown in Figures 6(a)–(c). In each figure, the rotating machine/structure mass ratio varies between 5 and 200 to cover relatively light and heavy weights of the machine. The mass ratio of the machine base mat and the rotating machine (m_{bR}/m_R), and the mass ratio of the floor and building base mat (m_i/m_{bs}) are both specified to be unity. These natural periods of the structure, 0.2, 1.0 and 2.0 s, are employed to cover the range of stiff and flexible structures. In addition, two friction coefficients, 0.20 and 0.01, are considered in this study.

Based on an extensive numerical study, in general, there are no noticeable changes in the peak disk response of various isolated systems as the mass ratios vary, except for a few cases of the rotor–RFBI–structure and the rotor–RFBI–structure–RFBI systems. Figure 6(a) shows that the disk acceleration responses of rotor–structure–RFBI remain roughly constant for the entire range of the mass ratio considered. From Figure 6(b), it is noticed that the peak disk response of the rotor–RFBI–structure system ($\mu_R = 0.2$; $T_s = 0.2$ s) fluctuates slightly as the mass ratio increases. The peak disk responses of the rotor–RFBI–structure system ($\mu_R = 0.01$; $T_s = 1.0$ s) have a dominant peak at mass ratio of 50 as well as a discrete upward jump at mass

Copyright © 2000 John Wiley & Sons, Ltd

ratio of 110 and leading to an almost constant peak response in mass ratio > 110 region. This peak response is due to resonance as the dominant frequency of the rotating machine is tuned to the natural frequency of the rotor–RFBI–structure system under this particular condition. From Figure 6(c), the peak disk response of the rotor–RFBI–structure–RFBI system ($\mu_R = \mu_s = 0.2$; $T_s = 0.2$ s) fluctuates in the low mass ratio region, but in general leads to an almost constant value

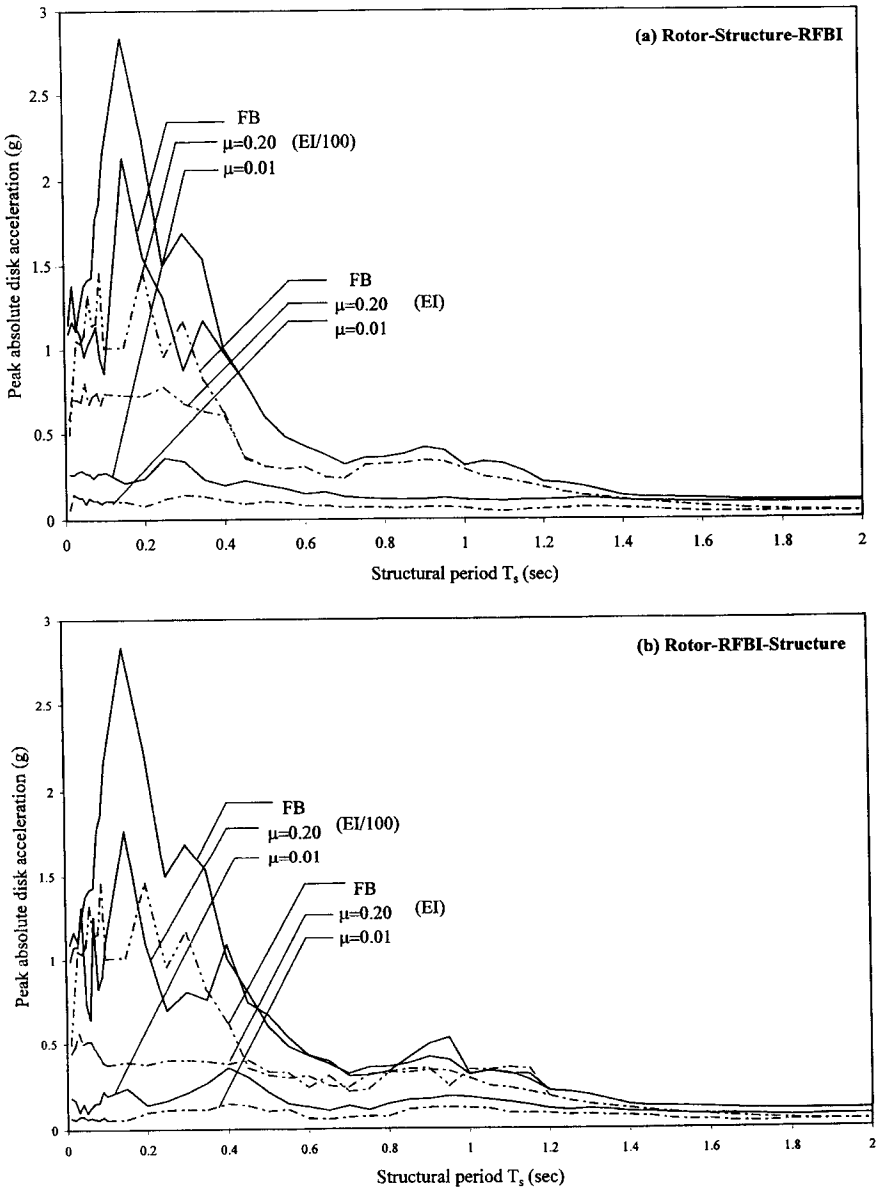

Figure 7. Effect of shaft rigidity on disk acceleration response.

Copyright © 2000 John Wiley & Sons, Ltd

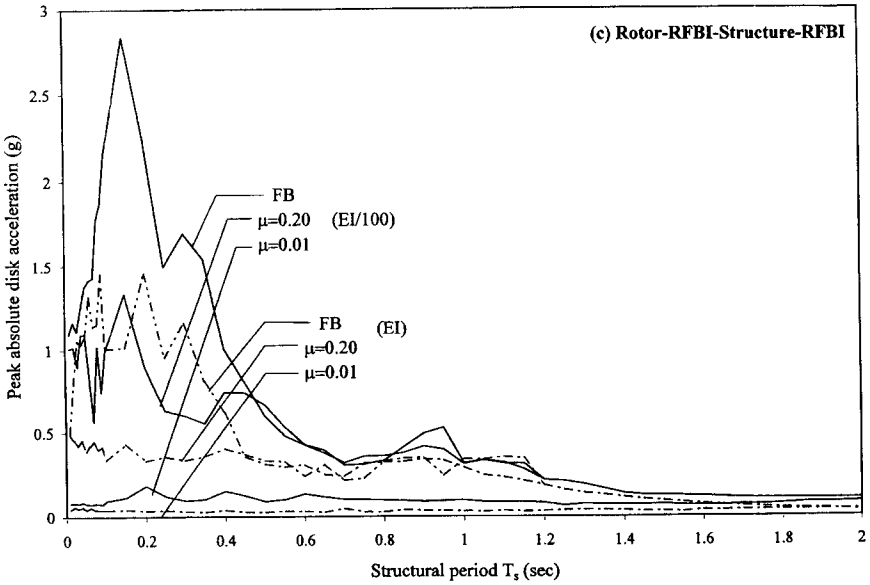

Figure 7. *Continued.*

in the high mass ratio region. Note that the peak disk response of the rotor–RFBI–structure–RFBI system ($\mu_R = \mu_s = 0.2$) at $T_s = 1.0$ s has higher response than that at $T_s = 0.2$ s in mass ratio >50 region. The peak disk response of the rotor–RFBI–structure system ($\mu_R = 0.01$) at $= 1.0$ s has larger response than that at $T_s = 0.2$ s in the mass ratio between 45 and 55 region. These imply that the high amplification period regions of the rotor–RFBI–structure–RFBI system $\mu_R = \mu_s = 0.2$) and rotor–RFBI–structure system ($\mu_R = 0.01$) are sensitive to variations in the mass ratio.

Effects of varying shaft flexibility, bearing rigidity and bearing damping

The effects of variations in shaft flexibility and bearing rigidity of the rotating machine on the disk response for the combined rotor–structure–RFBI system are shown in Figures 7 and 8, respectively. The shaft flexibility (EI) and bearing rigidity (K_{bearing}) are reduced by a factor of 100 to represent a relatively flexible shaft and bearing system, respectively. In each figure, the fixed-base case and the various isolated systems with two friction coefficients, 0.20 and 0.01, are considered.

From Figures 7(a)–(c) it is observed that increasing the flexibility of the shaft, in general, increases the absolute disk acceleration responses of the combined rotor–structure–RFBI systems. At the tuning period, $T_s = 0.15$ s, the disk acceleration responses of the relatively flexible shaft are reduced by factors of 1.33, 1.60 and 2.12 for the rotor–structure–RFBI, rotor–RFBI–structure and the rotor–RFBI–structure–RFBI models, respectively. This comparison indicates that the rotor–RFBI–structure–RFBI system is relatively very effective in reducing the disk response when the rotating components are subjected to strong ground motions such as the El Centro record. In the large amplification period region, $T_s < 0.4$ s, the disk acceleration

Copyright © 2000 John Wiley & Sons, Ltd

response spectra of the fixed-base and the various isolated systems with $\mu_R = \mu_s = 0.20$ cases are modified to a single dominant peak as the flexibility of the shaft increases. There are several exceptions where the disk acceleration responses in the isolated system exceed those in their corresponding fixed-base ones. This is due to the nonlinear slip-stick friction action at RFBI

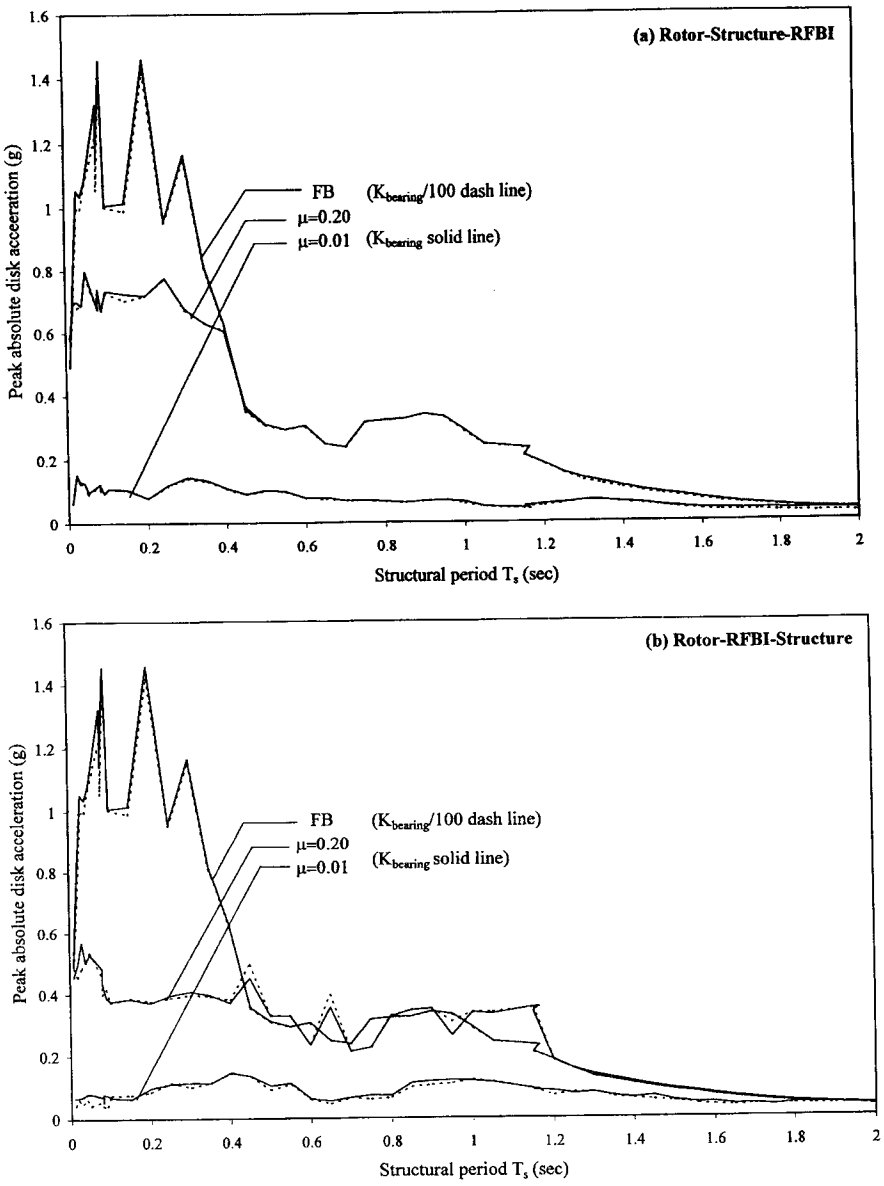

Figure 8. Effect of bearing rigidity on disk acceleration response.

Copyright © 2000 John Wiley & Sons, Ltd

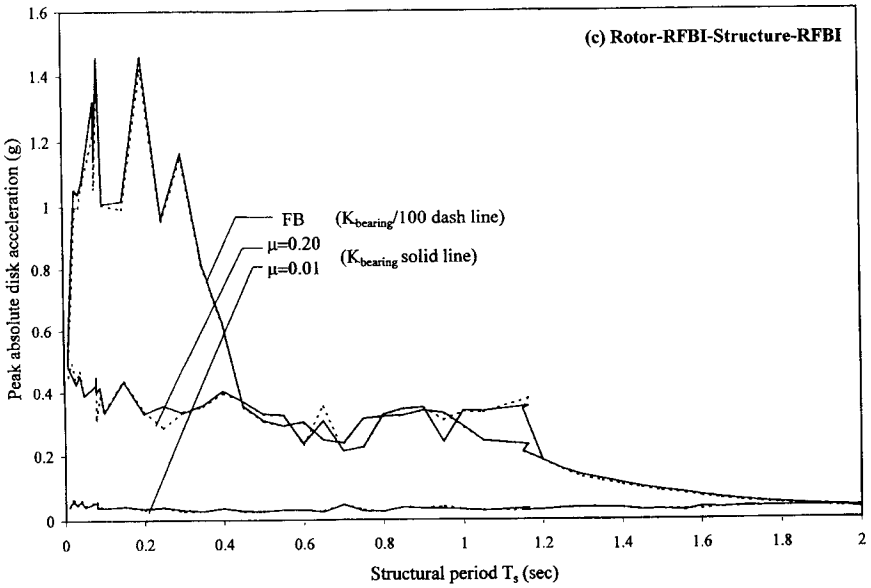

Figure 8. *Continued.*

system and coupled interaction forces described above. From Figures 8(a)–(c), it is noticed that the disk acceleration responses of the combined rotor–structure–RFBI systems are not noticeably decreased as the rigidity of the bearing system decreases, except those for the rotor–RFBI–structure model with $\mu_R = 0.01$.

The effect of variations in the bearing damping on the response of the rotating machine for the combined rotating machine–structure–RFBI systems is shown in Figure 9. Two damping values of the bearing system, $C_{bearing}/3$ and $C_{bearing}$ (bearing damping coefficient), are specified representing light damping and relatively heavy damping, respectively. Base friction coefficients of 0.01 and 0.20 representing two extremes of small and relatively large friction coefficients are considered.

The disk acceleration responses are reduced as the bearing damping increases for the fixed-base case and for the base-isolated cases of both friction coefficient values. Slight reductions in the large amplification responses occur as the bearing damping is increased. This indicates that bearing damping in the rotating machine is a potentially effective mechanism in reducing the peak disk response resulting from either the non-linear stick-slip friction action or the tuning region. In the high structural period region, however, varying the bearing damping has no noticeable effect on the disk responses in the combined rotating machine–structure–RFBI systems. There are several exceptions where the disk acceleration responses in the isolated systems exceed those in their corresponding fixed-base ones for both light and heavy bearing damping cases due to non-linear stick-slip action at the base isolators.

Note that, as shown in Equations (10)–(12), the bearing stiffness and damping coefficients are function of the speed of rotation. For certain values of speed of rotation, the real part of one of the system eigenvalues may become positive, leading to instability (unbounded disk responses). More insightful details of rotor stability will be discussed in the following section.

Copyright © 2000 John Wiley & Sons, Ltd

Effects of varying rotating speed

The natural frequency of the rotating system for a given constant speed of rotation can be obtained from the homogeneous equations of motion. An eigenvalue analysis of the equations of motion can be used to identify the critical speed at which the motion of the rotor will become unbounded.

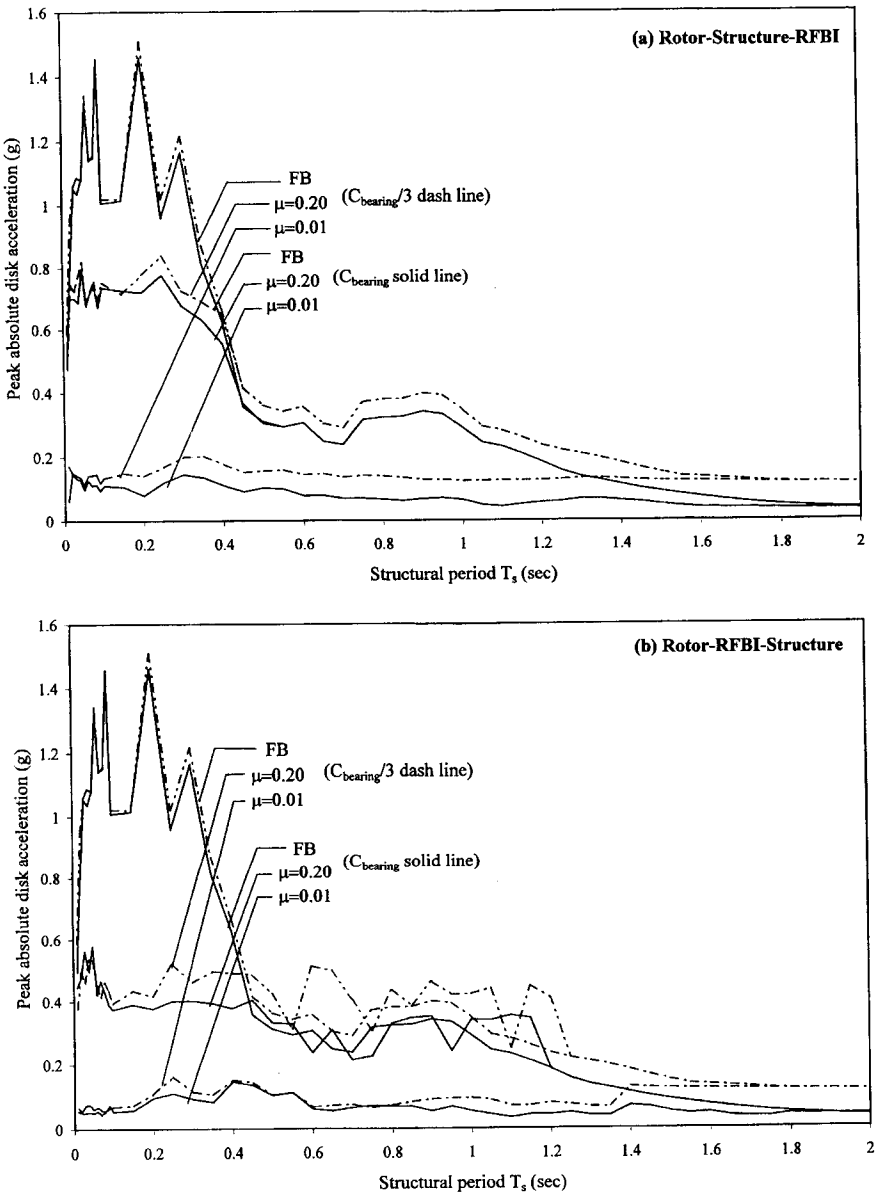

Figure 9. Effect of bearing damping on disk acceleration response.

Copyright © 2000 John Wiley & Sons, Ltd

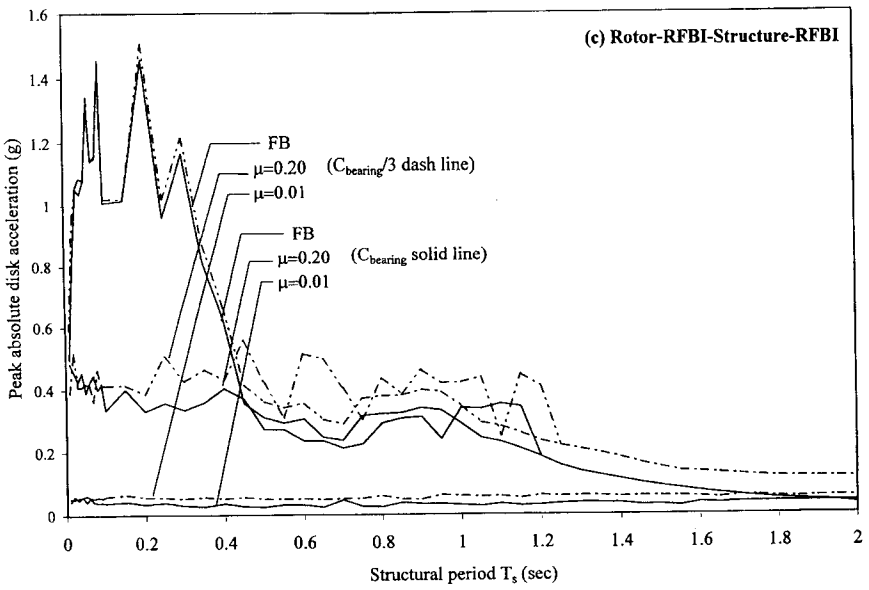

Figure 9. *Continued.*

The complex non-linear eigenvalue problem associated with the rotating machine located on the various base isolated system is

$$(\mathbf{M}\lambda^2 + \mathbf{C}\lambda + \mathbf{K}) \cdot \mathbf{x} = \mathbf{0} \tag{22}$$

where λ is an eigenvalue of the system and $\mathbf{x}$ is the corresponding eigenvector. This complex eigenvalue problem can be converted to a real linear problem by introducing an additional eigenvector $\mathbf{y}$ and solving the $2n \times 2n$ eigensystem (where n is the total number of degrees of freedom of the system),

$$\begin{bmatrix} \mathbf{0} & \mathbf{I} \\ -\mathbf{M}^{-1}\mathbf{K} & -\mathbf{M}^{-1}\mathbf{C} \end{bmatrix} \begin{Bmatrix} \mathbf{x} \\ \mathbf{y} \end{Bmatrix} = \lambda \begin{Bmatrix} \mathbf{x} \\ \mathbf{y} \end{Bmatrix} \tag{23}$$

where $\mathbf{M}$, $\mathbf{C}$ and $\mathbf{K}$ are the mass, damping and stiffness matrices of the complete system, respectively; and $\mathbf{I}$ is an identity matrix. The complex eigenvalues provide complete information about the system frequency ω and the corresponding modal damping ratio β, i.e.

$$\omega = |\lambda|, \quad \beta = -\operatorname{Re}(\lambda)/\omega \tag{24}$$

The primary cause of the instability of the rotor is caused by the asymmetric coefficients in the stiffness matrix due to the presence of the fluid-film bearings, even though the bearing system also provides desirable damping. If the motion of the rotor is stable, the real part of all eigenvalues must be non-positive, which implies that the modal damping ratios are zero or positive. To obtain the rotating speed at which the rotor becomes unstable, one can examine the largest real part of the system eigenvalues against the rotating speed.

Copyright © 2000 John Wiley & Sons, Ltd

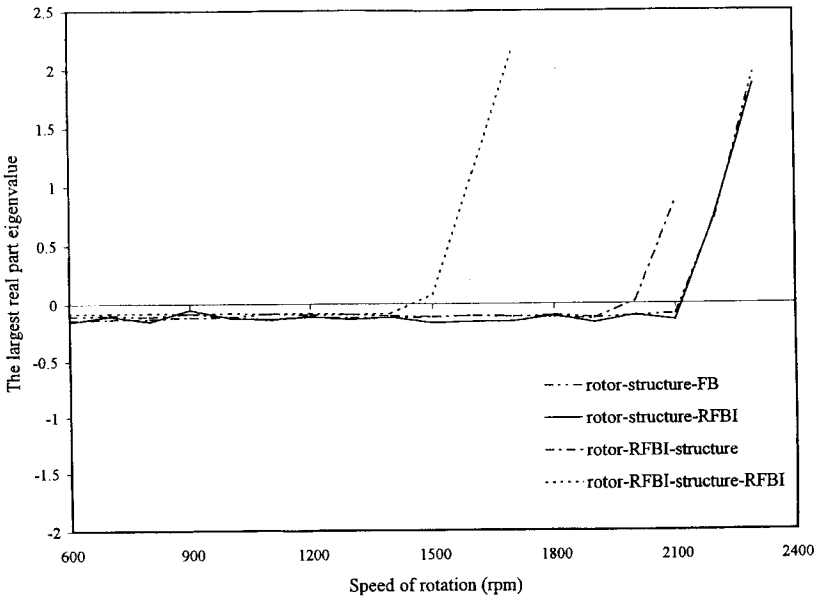

Figure 10. Variation in the largest real part of the system eigenvalues for the various RFBI systems with respect to speed of rotation.

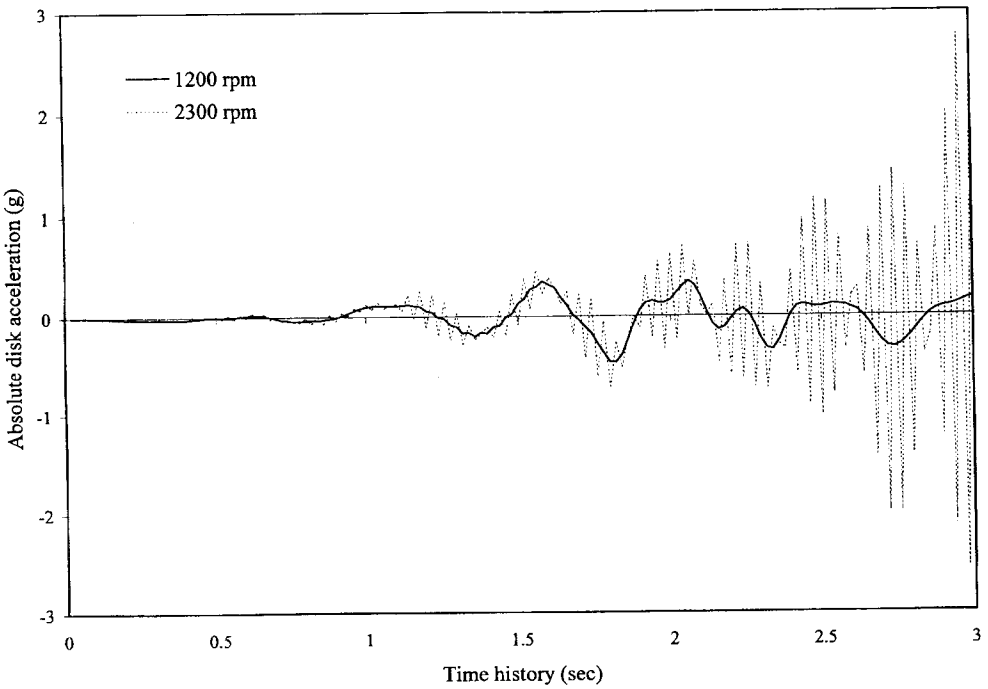

Figure 11. Time histories of disk acceleration operated at 1200 and 2300 rpm for the rotor–structure–RFBI system.

Copyright © 2000 John Wiley & Sons, Ltd

Variations in the largest real part of the system eigenvalues with respect to rotating speed are shown in Figure 10, which is obtained based on the assumption that the sign functions, $\mathrm{sgn}_R(\dot{s}_R)$ and $\mathrm{sgn}_s(\dot{s}_s)$, are $+1$. For the particular combination of system parameters used in this example, the figure shows that the critical speeds of rotation for the combined rotor–structure–RFBI systems are almost identical to that for the corresponding fixed-base system, except for the rotor–RFBI–structure–RFBI system.

For illustration, the rotor–structure–RFBI system with $\mu_s = 0.1$ and $T_s = 0.2$ s subjected to the El Centro earthquake is considered. The absolute disk acceleration response with operating speeds of 1200 and 2300 rpm are shown in Figure 11. Referring to Figure 10, one can observe a change from a negative to a positive value at the critical rotation speed of about 2150 rpm tends to be unbounded with increasing time, while the response of the system is stable at 1200 rpm.

CONCLUSIONS

The finite-element equations of motion for the rotating machines rested on a rigid base and the governing dynamic equations of motion for the combined rotating machine–structure–RFBI systems have been developed. The comparative results of an in-depth parametric study on the response of critical rotating machines located within the various isolated systems and the corresponding fixed base ones subjected to strong ground excitations have been presented. The influence of the isolator friction coefficient, rotating machine-to-structure mass ratio, shaft flexibility, bearing rigidity, bearing damping and critical rotating speed has been investigated.

Based on the numerical results presented in this study, the following general behaviours are observed.

(1) An increase in the friction coefficient increases the peak acceleration response and lowers the peak rotor sliding displacement for rotor–RFBI–structure model, but no systemic trend in peak rotor sliding displacement for rotor–RFBI–structure–RFBI model is observed. However, the influence of variations in the friction coefficient in the peak response of the system is rather gradual. For small friction coefficients, the spectral responses of the three base isolated systems appear to be almost independent frequency content of the excitation.

(2) Variations in the mass ratio $((m_{bs} + \sum_i m_i)/m_R)$, in general, have no significant effect on the peak disk response.

(3) An increase in the shaft flexibility (EI) or a decrease in the bearing damping (C_{bearing}) lead to an increase in the peak disk response. However, variations in the rigidity (K_{bearing}) of the bearing system appear to have no significant influence on the peak disk response.

(4) Instabilities of the rotating machines resting on various isolated configurations are primarily caused by the asymmetric stiffness terms of the fluid-film bearings. The coefficients of the bearing stiffness and damping depend on the speed of rotation, which implies that a rotating machine may become unstable at certain operating speeds. For a rotating machine to be stable, the real parts of the system eigenvalues must be negative (or at most zero). Conversely, the disk response becomes unbounded when the sign of the largest real part of the eigenvalues changes from negative to positive.

Copyright © 2000 John Wiley & Sons, Ltd

From this study, the relative performance and cost-effectiveness of the four models examined can be summarized as follow. The critical rotating machines rigidly attached to a floor within the structure can be protected from seismic damage by isolating the structure using the RFBI system (rotor–structure–RFBI). Alternatively to protect the rotating machine, the RFBI system can be directly applied to the base of the machine housed within a conventional (rotor–RFBI–structure) or an initially isolated structure (rotor–RFBI–structure–RFBI). In addition, considerable reductions in the level of peak disk acceleration response without introducing excessive sliding displacements at the bases of both machine and structure suggests that the RFBI system can be an effective device in protecting internal rotating components. However, if building cost is a major constraint in the design, additional seismic protection at the base of the rotating machine within an initially isolated structure (rotor–RFBI–structure–RFBI) may be unnecessary. This is because the rotor–structure–RFBI system already has impressive performance in reducing the floor seismic responses, consequently the maximum internal equipment seismic response will also be significantly reduced. For an existing conventional structure, the seismic protection of internal rotating machine can be achieved by adding either an RFBI system to the machine base (rotor–RFBI–structure) or retrofitting the existing structure (rotor–structure–RFBI).

APPENDIX

l	length of differential shaft element
ρ	mass density of flexible rotating shaft
A	cross-sectional area of flexible rotating shaft
m_d	mass of rigid disk
Ω	constant rotating speed of flexible rotating shaft
λ	system eigenvalue
ω	system frequency
β	modal damping ratio
E	Young's modulus
g	gravitational acceleration
n	total degrees of freedom of the system
N	specified floor of the multistorey building where the rotating machine is located
p	total number of floors in the multistorey building
s	local co-ordinate measured along the length of a finite element
s_f	Summerfield number
s_R, s_s	relative sliding displacements between the base mat of the rotating machine and a floor level, and between the base mat of the building and the ground, respectively
m_{bR}, m_{bs}	masses of the base mat of the rotating machine and structure, respectively
m_R, m_s, m_i	masses of the rotating machine, structure and ith floor, respectively
m_N, M_t	mass of the Nth floor and total mass of the system ($= m_R + m_{bR} + m_{bs} + \sum_i m_i$), respectively
μ, R	lubricant viscosity and journal radius of the journal-fluid-bearing system, respectively
w, h, D, L	weight on bearing, radial clearance, journal diameter and bearing length, respectively
u_x, u_y	relative displacements of differential shaft element in the x- and y-directions, respectively
θ_x, θ_y	rotations of the differential shaft element about x- and y-axes, respectively

Copyright © 2000 John Wiley & Sons, Ltd

$\ddot{x}_g, \ddot{y}_g$	horizontal and vertical components of the ground excitation, respectively
I_x, I_p	moment of inertia of flexible rotating shaft about the transverse and normal axes, respectively
I_t, I_o	moment of inertia of disk about the transverse and normal axes, respectively
ξ_{bR}, ξ_{bs}	damping ratios of the base isolator of the rotating machine and structure, respectively
ω_{bR}, ω_{bs}	natural circular frequencies of the base isolator of the rotating machine and structure, respectively
μ_R, μ_s	friction coefficients of the base isolator of the rotating machine and structure, respectively
$\mathbf{A}$	element matrix of rigid disk
$\mathbf{I}$	identity matrix
$\mathbf{q}$	vector of relative displacements of flexible rotating shaft with respect to its rigid base
$\mathbf{q}^e$	element vector of nodal displacements of flexible rotating shaft
$\mathbf{r}$	unit vector
$\mathbf{u}$	vector of relative displacements between a floor level and the building base mat
$\mathbf{y}$	additional eigenvector
$\mathbf{u}^e, \boldsymbol{\phi}^e$	vectors of relative displacements an rotations for a typical shaft element, respectively
$\mathbf{N}, \mathbf{N}'$	matrices of interpolation function and its first derivation with respect to s, respectively
$\mathbf{e}_1, \mathbf{e}_2$	operational vectors
$\mathbf{M}, \mathbf{M}^s, \mathbf{M}^R$	mass matrices of the isolated system, structure and rotating machine, respectively
$\mathbf{M}_s^e, \mathbf{M}_d^e$	element mass matrices of flexible rotating shaft and rigid disk, respectively
$\mathbf{C}, \mathbf{C}^s, \mathbf{C}^R$	damping matrices of the isolated system, structure and rotating machine, respectively
$\mathbf{C}_s^e, \mathbf{C}_d^e, \mathbf{C}_b^e$	element damping matrices of flexible rotating shaft, rigid disk and bearing system, respectively
$\mathbf{K}, \mathbf{K}^s, \mathbf{K}^R$	stiffness matrices of the isolated system, structure and the rotating machine, respectively
$\mathbf{K}_s^e, \mathbf{K}_d^e, \mathbf{K}_b^e$	element stiffness matrices of flexible rotating shaft, rigid disk and bearing system, respectively
$\mathbf{f}^R(t)$	applied force vectors of the rotating machine
$\mathbf{f}_s^e(t), \mathbf{f}_d^e(t)$	element applied force vectors of flexible rotating shaft and rigid disk, respectively
$\mathbf{a}_b(t)$	vector of transitional base accelerations

ACKNOWLEDGEMENTS

Partial financial support from the U.S. National Science Foundation under Grant No. CMS-9301464 and the Department of Civil, Construction and Environmental Engineering at Oregon State University is gratefully acknowledged.

REFERENCES

1. Kelly JM. Base isolation: linear theory and design. *Earthquake Spectra* 1990; **6**:233–243.
2. Srinivasan V, Soni AH. Seismic analysis of a rotating mechanical systems — a review. *Earthquake Engineering and Structural Dynamics* 1982; **14**(6):13–19.
3. Srinivasan V, Soni AH. Seismic analysis of a rotor-bearing system. *Earthquake Engineering and Structural Dynamics* 1984; **12**:287–311.

Copyright © 2000 John Wiley & Sons, Ltd

4. Suarez LE, Singh MP, Rohanimanesh MS. Seismic response of rotating machines. *Earthquake Engineering and Structural Dynamics* 1992; **21**:21–36.
5. Su WC. Dynamic response of flexible rotating machines subjected to ground excitations. *Master of Science Thesis*, Department of Civil Engineering, Oregon State University, Corvallis, OR, 1994.
6. Su WC, Hernried AG. Seismic response of flexible rotating machines. *7th Canadian Conference on Earthquake Engineering*, Montreal, 1995; 229–236.
7. Kelly JM. Aseismic base isolation. *Shock Vib. Dig.* 1982; **14**:17–25.
8. Kelly JM. Aseismic base isolation: review and bibliography. *Soil Dynamics in Earthquake Engineering* 1986; **5**:202–216.
9. Mostaghel N, Khodaverdian M. Seismic response of structure supported on RFBI system. *Earthquake Engineering and Structural Dynamics* 1988; **16**:839–854.
10. Gueraud R, Noel-Leroux J-P, Livolant M, Michalopoulos AP. Seismic isolation using sliding-elastomer bearing pads. *Nuclear Engineering Design* 1985; **84**:363–377.
11. Mostaghel N, Tanbakuchi J. Response of sliding structures to earthquake support motion. *Earthquake Engineering and Structural Dynamics* 1983; **11**:729–748.
12. Kelly JM, Beucke KE. A friction damped base isolation system with fail-safe characteristics. *Earthquake Engineering and Structural Dynamics* 1983; **11**:33–56.
13. Chen D, Clough EW. Earthquake response of structure with friction sliding motion. Earthquake Engineering Research Center, University of California, Berkeley, CA, 1981.
14. Younis CJ, Tadjbakhsh IG. Response of sliding rigid structure to base excitation. ASCE, *Engineering Mechanics* 1984; **110**:417–432.
15. Constantinou MC, Tadjbakhsh IG. Response of a sliding structures to filtered random excitation. *Structural Mechanics* 1984; **12**:401–418.
16. Mostaghel N, Khodaverdian M. Dynamics of resilient-friction base isolator (RFBI). *Earthquake Engineering and Structural Dynamics* 1987; **15**:379–390.
17. Mostaghel N. Resilient-friction base isolator. *Report No. UTEC 84-097*, University of Utah, 1984.
18. Kelly JM, Hodder SB. Experimental study and elastomeric damper for base isolation systems in laminated neopreme bearings. *Bulletin of the New Zealand National Society for Earthquake Engineering* 1982; **15**:53–67.
19. Kelly JM, Skinner MS, Beucke KE. Experimental testing for an energy absorbing base isolation system. *Report No. UCB/EERC-80/35*, Earthquake Engineering Research Center, University of California, Berkeley, CA, 1981.
20. Hernried AG, Lei KM. Semi-Analytical Techniques for the determination of the dynamic response of equipment in structures supported on coulomb friction elements. *Earthquake Engineering and Structural Dynamics* 1995; **24**:801–810.
21. Ahmadi G, Su L. Equipment response spectra for base-isolated shear beam structures. *Nuclear Engineering Design* 1992; **132**:287–308.
22. Hernried AG, Lei KM. Parametric studies on the response of equipment in resilient-friction base isolated structures subjected to ground motion. *Engineering Structures* 1993; **15**:349–357.
23. Rao JS. *Rotor Dynamic*. Wiley: New Delhi, 1983.
24. Earles LL, Palazzolo AB. Hybrid finite element — boundary element simulation of rotating machinery supported on flexible foundation and soil. *Rotating Machinery Dynamics* 1987; **2**:371–381.
25. Pinkus O, Sternlicht B. *Theory of Hydrodynamic Lubrication*. McGraw-Hill: New York, 1961.
26. Lund JW, Tomsen KK. A calculation method dan daat for the dynamic coefficients of oil-lubricated journal bearing. In Topic in Fluid Film Bearing and Rotor Bearing Systems Design and Optimization. ASME, *Design Engineering Conference*, Chicago, IL, 1978; 1–28.
27. Lund JW. Calculation of stiffness and damping properties of gas bearings lubrication technology. ASME, *Journal of Transportation*, Series F 1968; **90**:793–803.
28. Newmark NM. A method of computation of structure dynamic. ASCE, *Engineering Mechanical Division* No. EM3 1959; **85**:67–94.
29. Mostaghel N, Hejazi M, Tanbakuchi J. Response of sliding structures to harmonic support motion. *Earthquake Engineering and Structural Dynamics* 1983; **11**:355–366.

Copyright © 2000 John Wiley & Sons, Ltd